Temperature Dependent Characteristics of La_2O_2S: Ln [Ln=Eu, Tb] with Various Ln Concentrations over 5 – 60 ˚C.

Sook Voon Yap*, Robert M. Ranson, Wayne M. Cranton, Demosthenes C. Koutsogeorgis, Gary B. Hix

School of Science and Technology, Nottingham Trent University, Nottingham.

NG11 8NS.United Kingdom.

Sook Voon Yap*

Nottingham Trent University

School of Science and Technology

Clifton Lane, Nottingham.

NG11 8NS. United Kingdom.

Tel : +44 (0)1158483163

E-mail : sook.yap@ntu.ac.uk

Abstract

This research is aimed at developing an optical sensor for remotely measuring human skin temperature in electromagnetically hostile environments, such as within a magnetic resonance imaging (MRI) scanner. In this feasibility study, various concentrations of europium doped lanthanum oxysulphide (La_2O_2S: Eu- 0.1-15 mol % (m/o)) and terbium doped lanthanum oxysulphide (La_2O_2S: Tb - 0.005-50 m/o) have been investigated in terms of crystallinity, photoluminescent (PL) spectral and decay time characteristics. For both phosphors, X-ray diffraction (XRD) has shown that as dopancy increases, the (100) and (002) reflections merge and there is a reduction in the *c*-axis parameter as well as the crystallite size. Photoluminescent characterisation (337 nm excitation) has also shown a dependency to dopant concentration through variance of peak intensity. Temperature dependent decay time measurements were carried out over a low temperature range of 5 to 60 °C. Optimum brightness of these temperature dependent lines is achieved at concentrations of 1 and 10 m/o for La_2O_2S: Eu and La_2O_2S: Tb respectively. However, optimum temperature dependency is achieved at lower concentration for La_2O_2S: Eu, specifically at 0.1 m/o. In comparison to conventional phosphor temperature dependent characteristic, La_2O_2S: Tb showed an increase in decay time with respect to temperature for concentrations above 2 m/o.

PACS codes: 33.50. Dq; 33.50. –j; 07.07.Df; 78.55.-m

Keywords: Phosphors; photoluminescence; decay time; temperature sensing; quenching rate; X-ray diffraction

Introduction

Over the last several decades, thermographic phosphors have been extensively explored for remote temperature sensing measurement. This is attributed to their accurate sensing capability over a wide range of temperatures, as well as their ability to withstand a harsh environment. For example, europium doped yttrium oxide (Y_2O_3: Eu) has been utilised for high temperature sensing within a rotating gas turbine[1, 2] and magnesium fluorogermanate doped with manganese ($Mg_4(F)GeO_6$: Mn) has been explored for thermal mapping of hot spots on the walls of a cryogenic fuel tank[3]. Problems associated with temperature monitoring within a magnetic resonance imaging (MRI) scanner, particularly to an infant or a critical-care patient, has provided an impetus for the development of a phosphor-based optical sensor for human skin temperature sensing (27- 37 °C[4, 5]) within such an environment. A desired optical sensor using the decay rate of luminescence from a thermographic phosphor could therefore be the ideal temperature sensing tool for this delicate application due to the fact that thermographic phosphor thermometry is independent of external triggering source and electromagnetic interference. However, the potential issues such as thermal conductivity and the length of contact time between the human skin and the bonding of the phosphor will be taken into consideration at a later stage of the sensor design. In this work, two potential phosphors have been selected for use within the desired optical sensor, namely La_2O_2S:

Eu and La_2O_2S: Tb. The results indicate that both of the phosphors are temperature dependent over 5-60 °C.

The crystallite size of the phosphors plays an important role in determining the changes in decay rates. At Nottingham Trent University (NTU), the crystallite size and crystallinity of La_2O_2S: Eu (0.1-15 mol% (m/o)) and La_2O_2S: Tb (0.005-50 m/o) have been characterised by X-ray diffraction (XRD) and the measurements were concentrated on the (100) and (002) planes. As dopancy increases, the observed peaks merge and the XRD analysis has shown a reduction in the crystallite size and the *c*-axis of the (002) plane. In addition, photoluminescent (PL) results also demonstrate a change in the relative emission intensities at various dopancy levels. This is due to the electronic transitions occurring between the discrete levels of ^5D to ^7F levels of the dopant ions sited in the crystal lattice in relation to the Stark effect[6]. The quenching concentrations for both phosphors are encountered when the optimum brightness for the temperature dependent lines is achieved.

Typically, temperature dependent characteristics of a thermographic phosphor can be explored by decay time and two-peak intensity[7]. In this research, decay time is the preferred approach as it is independent of the excitation source and ambient light. The decay time of luminescence can be deduced according to the relation,

Equation 1: $I(t) = I_O \exp(-\frac{t}{\tau})$

(where I(t) = intensity at time t, I_0 = initial intensity at time 0 and τ = decay time)[8].

It should be noted that the decay profiles presented in this paper were fitted with the standard single exponential decay equation providing goodness of fit (r^2) > 99.5%. A double exponential decay relationship was also attempted but resulted in a less accurate fit (r^2 < 90%) with both decay times being within 5% of each other.

Simons et al. [9] also describes the decay time of a phosphor as being strongly dependent on its temperature. The expression is:

Equation 2: $\tau_d = \tau_q \exp\left(-Q(T - T_Q)\right)$

(where the decay constant (τ_d) is related to the component temperature (T) above the quenching point (T_Q); τ_q is the decay time at the quenching point; and the quenching rate Q is the rate at which the decay time varies with temperature). Therefore the quenching rate is directly related to the sensitivity of a phosphor; the higher the quenching rate the more sensitive a phosphor is to temperature variation. The decay time results presented in this paper indicate that both of La_2O_2S: Eu and La_2O_2S: Tb are highly sensitive with notable quenching rates over 5-60 °C. More importantly, this paper shows an unprecedented decay time characteristic, namely, the decay time for La_2O_2S: Tb at higher dopant concentrations (>2 m/o) increases as a function of temperature.

Experimental Procedures

The powdered phosphors, La_2O_2S: Eu (SKL63/ F-R1) and La_2O_2S: Tb (SKL65/ N-C1) were supplied by Phosphor Technology Ltd (PTL). These polycrystalline powder phosphors at various dopant concentrations were examined using the Philips X'Pert Pro XRD system with monochromated Cu-$K_{\alpha 1}$ radiation, λ = 1.54056 Å (45 kV, 40 mA operating mode). To ensure the studied data was self-consistent, XRD measurements for different concentrations of a specific phosphor were carried out on the same day and a Silicon standard was used as a control sample allowing repeatability. Experiments were therefore concentrated on the $25° \leq 2\theta \leq 27°$ Bragg angles consisting of the (100) and (002) reflections which will give the variation in the *c* cell parameter with dopant concentration. The data were collected with 0.008° step size and a count time of 150 seconds per step.

To enable decay time and PL measurements to be made, the phosphor powders have been compressed to form a pellet (5 mm diameter, 2 ± 0.5 mm thick) so that it could be mounted within a digitally controlled incubator (IPP 200). A calibrated T-type thermocouple was attached at the back of the sample and the temperatures were measured using a PicoLog TC-08 data logger. The comparison of the controlled and measured temperatures showed an accuracy of +- 0.1 ˚C over the working temperature

range.

The excitation spectra for La_2O_2S: Tb and La_2O_2S: Eu provided by PTL indicate that the excitation wavelength at 337 nm is sufficient enough to illuminate both of the phosphors. A pulsed nitrogen (N_2) laser (VSL-337ND) was used as an UV excitation source which emits 337 nm with a 4 ns pulse length. The laser beam is guided to the sample by a mirror. The resulting fluorescence was consequently collected by a quartz rod and transmitted to a monochromator (DMC1-03, Optometrics LLC.), thus restricting the emission to a 3 nm bandwidth at the detector – a photomultiplier tube (PMT 9558QB). The PMT converted the detected decay signal into an electrical waveform via an oscilloscope (Gould DSO 4072) for subsequent analysis. In order to enhance the signal-to-noise ratio, the noise reduction was performed by digitally averaging the signals over a period of one minute and this equates to 1200 decay rate signals. The decay time was always measured from the same time window (3-5 μs after the 4 ns laser excitation pulse) with the single exponential equation for comparison purposes. For the standard PL spectra set-up, an optical fibre is utilised to transmit the fluorescence signal to a spectrometer (S2000, Ocean Optics Inc (OOI)) and the acquired spectrum can be interpreted via OOI software.

Results and Discussion

i. X- Ray Diffraction (XRD)

XRD patterns of La_2O_2S: Tb and La_2O_2S: Eu over the diffraction angles of $5° \leq 2\theta \leq 55°$ is shown in Figure 1. These match the reference pattern (PDF code: 00-027-0263) of the parent compound La_2O_2S. This indicates that the hexagonal crystal structure of La_2O_2S is consistent in the doped materials and its crystal lattice parameters lie within the interval of $3.41 < a < 3.51$ Å and $6.79 < c < 6.94$ Å (the *a*-axis and *c*-axis of a unit cell[10]).

The shift in 2θ of the (200) reflection with an increase in the Tb dopancy level is mainly due to the variations in the crystal lattice, i.e. *c*-axis shrinks with increasing Tb concentration as seen in Figure 2. This is based on the size of the ionic radius of both La (102 pm) and Tb (92 pm) in the unit cell, which decreases as the Tb concentration becomes dominant. With increasing Tb concentration, the two individual peaks at 25.52° ((100) reflection) and 25.78° ((002) reflection) merge gradually and eventually form a broad peak at 50 m/o Tb. This merging behavior alters the formation of the crystal lattice and hence produces a multitude of probability of occurrence for both radiative and non-radiative transitions. There is little change at low concentrations (<1 m/o) and the data fit the pseudo-linear relationship as demonstrated in Figure 3. In addition, the crystallite size of La_2O_2S: Tb decreases owing to a reduction in the volume

of the unit cell with increasing Tb dopancy. By using the Scherrer equation, which relates the width of peaks in an X-ray powder diffraction pattern to crystal size, the crystallite size of the phosphors can be determined as tabulated in Table 1.

Figure 4 indicates the *c*-axis variations in the position of the (002) reflection peaking at 25.612° as a function of Eu concentration. This has illustrated a pseudo-linear relationship between the Eu concentration and a shift in the position of this peak to smaller values of 2θ. These data are consistent since Eu has an ionic radius of 95 pm which is smaller than La (102 pm), and hence an expected decrease in the volume of the unit cell occurs as Eu dopant concentration becomes significant.

The variation of the crystallite size of La_2O_2S: Eu is shown in Table 2. The host lattice La_2O_2S has the biggest crystallite size which is about 0.16 μm than that of the other Eu doped La_2O_2S. The crystallite size of La_2O_2S: Eu has reduced to 2.5 times smaller than the host lattice. In addition, results at NTU showed that the commonly investigated La_2O_2S: Eu at higher concentrations with smaller crystallite size has a faster decay rate against temperature as demonstrated in Fig 9 (a) – (d). On the other hand, Fig 11 also illustrate that the decay rates for La_2O_2S: Tb with smaller crystallite size are faster than those of larger crystallite size at lower concentrations. For >2 m/o Tb, an interesting trend was evident showing an increase in the decay time with temperature.

However, the quenching rates for these phosphors at low dopant concentrations (large crystallite size) are greater than high dopant concentrations (small crystallite size) implying that they are more sensitive to temperature variance and hence a relationship between dopant concentration and decay time is established: a phosphor with lower concentration shows a better temperature dependency.

Table 1 Crystallite size of 0-50 m/o La_2O_2S: Tb.

Dopant Concentrations (m/o)	Crystallite size (Å)
0	1560
0.005	1324
0.2	1464
0.5	1416
1	1416
2	1448
5	1077
10	997
15	993
20	904
30	834
40	783
50	888

Table 2 Crystallite size for various concentrations of La_2O_2S: Eu.

Dopant Concentrations (m/o)	Crystallite size (Å)
0	1579
0.1	1020
1	1053
2	1015
5	891
7.36	833
10	643
15	656

ii. **Spectral data**

The emission spectrum of La_2O_2S: Tb is determined by the transitions of electrons from an upper ($^5D_3$) and a lower ($^5D_4$) excited level to the level of the multiplet term ^7F_J (J= 0, 1, 2, 3, 4, 5, 6) levels of the $4f^8$ configuration[11, 12]. The emission of terbium-doped phosphor is mainly in the green due to transitions $^5D_4 \rightarrow {}^7F_J$ and the blue emission contributes to the emission from the higher level transitions $^5D_3 \rightarrow {}^7F_J$[12]. At lower Tb concentrations of less than 0.5 m/o, the phosphor emits orange at 0.5 m/o, then red at 0.2 and 0.005 m/o. At low concentrations (≤0.5 m/o), more peaks are produced in the emission spectrum due to the Stark effect[6] and the dominant peak has shifted from the green line 544 nm to the red region peaking at 624 nm as indicated in Figure 5. The high terbium concentrations (≥ 0.92 m/o) exhibit six solid emission peaks at 489 nm, 493 nm, 544 nm, 548 nm, 587 nm and 621 nm. These peaks showed temperature dependencies with fast decay time.

For emission wavelengths in the green region (489- 548 nm), Tb concentration reached a quenching point at 10 m/o Tb as it has the optimum intensity emission as seen in Figure 6. On the other hand, the red region (≥ 587 nm) is dominated by low terbium concentrations.

The emission spectra of La_2O_2S: Eu were characterised over a dopant concentration range from 0.1 to 15 m/o of Europium. Figure 7 illustrates the intensities of the

emission peaks vary with various dopant concentrations. Low dopant concentrations of Eu (≤ 2 m/o) appear to have more emission lines especially at the shorter wavelengths, such as 467 nm and 495 nm. In addition, the shorter wavelength lines at low Eu concentrations are far more intense than they are at higher concentrations. The increase number of these emission lines in the spectrum is due to the Stark Splitting effect[6] of discrete energy levels between ^5D levels to ^7F levels [13]. It is important to note that these peaks at short wavelengths are temperature dependent and hence they could be used for remote temperature measurements.

Shown in Figure 8 is the intensity graph of La_2O_2S: Eu over a number of dopant concentrations. This clearly shows that concentrations of 1-2 m/o of Eu achieving the maximum intensity emission particularly at the temperature dependent peaks and thus they are the optimum concentrations for this phosphor. A reduction of these emission peaks occurs for 5-15 m/o Eu due to the concentration quenching[14].

iii. **Decay time characteristics**

Figure 9 (a) – (d) demonstrate the decay time characteristics of La_2O_2S: Eu 0.1-15 m/o within a temperature range of 5-60 °C. Decay time characteristics were measured at the temperature dependent wavelengths of 467 nm, 495 nm, 512 nm and 538 nm. These transitions that occur between the ^5D levels and charge transfer states (CTS) of La_2O_2S:

Eu can be described with the model developed by Fonger and Struck [9, 15]. Their analysis suggested the Eu ^5D_J states quench sequentially (J= 3, 2, 1, 0) with increasing temperature. This is because each ^5D state empties thermally via charge transfer.

Due to the constraint of the spectrometer resolution and its sensitivity, only the 467 nm and 495 nm are visible in lower concentrations of Eu (≤ 2 m/o) as shown in Figure 7b (see inset). These lower emission intensity peaks could be detected at other dopant concentrations via decay time system due to the improved sensitivity of the PMT in comparison with the spectrometer's CCD array. Results presented here show the decay time of these samples decreases with an increasing temperature. At low temperatures, the decay rate for 467 nm, 495 nm and 512 nm is ~10^{-6} s whereas 538 nm has a slower decay rate of ~ 10^{-5} s. For comparison, Cates and Allison [13] reported the decay time of 512 nm line was 6.2 μs.

The data summarised in Table 3 indicate that 0.1 m/o Eu has the most superior quenching rates of 20.92 m°C^{-1}, 24.03 m°C^{-1}, 22.23 m°C^{-1} at 467 nm, 495 nm and 512 nm respectively. In addition, a trend is clearly illustrated with the quenching rates decreasing as dopancy levels increase for these highly temperature-sensitive peaks. Although the emission from 1-2 m/o Eu are more intense, the quenching rates for these two dopancy levels are still lower than that of 0.1 m/o. It is hypothesized that the

quenching rates are independent of the brightness of a phosphor but dependent on the dopant concentration as discussed earlier. As a result, 0.1 m/o Eu would be the ideal candidate for embedding within an optical temperature sensor.

Table 3 Summary of quenching rates for various concentrations of La_2O_2S: Eu.

Emission wavelengths (nm)	Quenching rates ($m°C^{-1}$) of La_2O_2S: Eu						
	0.1 m/o	1 m/o	2 m/o	5 m/o	7.36m/o	10 m/o	15 m/o
467	20.92	13.73	14.64	16.16	10.36	8.50	4.90
495	24.03	17.10	16.71	14.60	8.70	5.28	5.41
512	22.23	19.84	17.08	14.80	9.90	6.53	6.02
538	1.77	2.27	2.00	3.12	2.84	0.85	1.36

Various investigations have explored the temperature sensing capabilities of La_2O_2S: Tb. The results obtained in this work have suggested that the decay times of this phosphor show strong dependency upon its temperature, as indicated in Figure 10-Figure 11. Of more importance, this temperature dependent characteristic occurs at most of the emission intensities in La_2O_2S: Tb, i.e. $^5D_4$ to ^7F_J transitions [16] compared to only four emission lines of La_2O_2S: Eu. According to Struck and Fonger, again similar to La_2O_2S: Eu, the thermal quenchings of Tb in La_2O_2S are due to the CTS crossover relaxation to Frank-Condon shifted states.

Like many other cases, the decay time of La_2O_2S: Tb 0.005- 0.91 m/o decreases with temperature. However, it is observed that 5-50 m/o Tb showed an unprecedented decay time characteristic: its decay time increases with temperature. A good example of this abnormal decay time behavior is shown in Figure 10, the decay time of 544 nm at 5 °C

is 269 μs whilst 371 μs at 60 °C. As the dopant concentration is increased, it will result in a change of crystal structure and hence an alteration to the energy levels that exist for excited states (Stark-splitting effect). It would appear that this has induced a trapping state and/or additional energy levels which result in phonon rather than photon emission. This would have two effects - reduction of intensity and an observed slow-down of the luminous decay process, due to the excited states now relaxing to an intermediate state before reaching the photon relaxation energy level.

The quenching rates of La_2O_2S: Tb are presented in Table 4.Unlike the steep quenching slopes of La_2O_2S: Eu, the average quenching rate of La_2O_2S: Tb is as low as ~ 3 $m°C^{-1}$ with faster decay times depending on the Tb concentrations and also the emission peak.

In summary, the most superior quenching rates at those temperature dependent peaks appear to be at the lowest dopant concentration of the phosphors investigated, i.e. 0.005 m/o La_2O_2S: Tb and 0.1 m/o La_2O_2S: Eu. Further charaterisation of both phosphors at even lower dopancy level will be carried out to validate the relationship between concentration of the activators and quenching rates.

Table 4 Quenching rates of different Tb concentrations at all emission peaks. (The negative sign (-) is used to denote the increase decay times with increasing temperature.)

Emission wavelengths (nm)	Quenching rates (m°C-1) of La_2O_2S: Tb				
	0.005 m/o	0.91 m/o	2 m/o	10 m/o	50 m/o
467	2.79				
490	2.49	2.10	-2.97	-1.85	-1.12
493	3.29	2.39	-1.81	-2.14	-1.47
512	4.66				
531	3.36				
538	1.39				
544	3.90	3.19	-1.18	-2.01	-1.32
548		3.56	-1.10	-2.42	-0.80
555	4.19				
563	3.63				
587	2.35	4.73	-0.11	-1.58	-1.00
594	4.92				
615	3.28				
621	2.08	4.65	2.53	-1.82	-0.46

Conclusions

The XRD analysis, spectral data and decay time results of powdered La_2O_2S: Eu and La_2O_2S: Tb showed these phosphors to be suitable for the fabrication of the desired optical sensor. Dopant concentration is a key factor that has be taken into account for the measurements described above. The results showed significant changes in crystallinity, emission intensities and decay rates with various dopant concentrations over 5-60 °C. The most sensitive temperature sensing phosphor discovered in this work is 0.1 m/o La_2O_2S: Eu with a great quenching rate of ~20 $m°C^{-1}$ at its temperature dependent lines.

A new decay time trend is introduced at NTU, a rise in decay time with an increasing temperature was evident over dopant concentrations of 2-50 m/o La_2O_2S: Tb. This is due to a distortion of the crystal field associated with the amount of the dopant introduced to the lattice which causes the splitting of energy levels, and thus increase the probability of occurrence for the radiative and non-radiative transitions.

In addition, a relationship between dopant concentration and decay time has been established for La_2O_2S: Eu and La_2O_2S: Tb over various dopancy levels. Lower dopant concentration phosphors with larger crystallite size induced a slower decay rate but a higher quenching rate, suggesting they are more superior in temperature sensing to a higher dopant concentration phosphor.

Acknowledgement

The authors acknowledge the financial support from The Engineering and Physics Sciences Research Council (EPSRC).

References

[1] R. M. Ranson, C. B. Thomas and M. R. Craven, *Journal of Measurement Science and Technology* **1998**, *9*, 1947-1950.

[2] R. M. Ranson, E. Evangelou and C. B. Thomas, *Applied Physics Letters* **1998**, *72*, 2663-2664.

[3] D. L. Beshears, G. J. Capps, C. M. Simmons and S. W. Schwenterly in *Laser-induced fluorescence of phosphors for remote cryogenic theromometry* **1990**

[4] L. Jansky, V. Vavra, P. Jansky, P. Kunc, I. Knizkova, D. Jandova and K. Slovacek, *Journal of Thermal Biology* **2003**, *28*, 429-437.

[5] G. Wasner, J. Schattschneider and R. Baron, *Journal of Pain* **2002**, *98*, 19-26.

[6] J. S. Foster, *Journal of the Franklin Institute* **1930**, *209*, 585-588.

[7] S. W. Allison and G. T. Gillies, *Review of Scientific Instruments* **1997**, *68(7)*, 2615-2650.

[8] S. Shionoya and W. M. Yen, *Phosphor handbook*, CRC Press LLC **1998**

[9] A. J. Simons, I. P. McClean and R. Stevens, *Electronics Letters* **1996**, *32*, 253-254.

[10] P.J.Brown and J.B.Forsyth, *The Crystal Structure of Solids*, Edward Arnold Limited **1973**

[11] A. M. Amiryan, A. M. Gurwich and R. V. Ktomina, *Journal of Applied Spectroscopy* **1977**, *27*, 468-472.

[12] G. Blasse and B. C. Grabmaier, *Luminescent Materials*, Springer-Verlag Berlin Heidelberg, **1994**

[13] M. B. Cates, S. W. Allison, L. A. Franks, M. A. Nelson, T. J. Davies and B. W. Noel, (Laser Institute of America) **1984**

[14] S. Ignasiak and H. Veron, *Journal of the Electrochemical Society* **1976**, *123*, 1493-1497.

[15] W. H. Fonger and C. W. Struck, *Journal of the Electrochemical Society* **1971**, *118*, 273-280.

[16] C. W. Struck and W. H. Fonger, *Journal of Applied Physics* **1971**, *42*, 4515-4516.

Figure Captions

Figure 1 XRD patterns of La_2O_2S: Tb and of La_2O_2S: Eu at room temperature.

Figure 2 XRD patterns at 0.005% and 50% Tb dopancy levels over $25° \leq 2\theta \leq 26.5°$.

Figure 3 *C*-parameter of a unit cell of La_2O_2S: Tb and La_2O_2S: Eu as a function of dopant concentration at (002) reflection.

Figure 4 XRD patterns of La_2O_2S: Eu at different dopancy levels.

Figure 5 Emission spectra comparison of La_2O_2S: Tb at 0.2 m/o and 10 m/o Tb contents under 337 nm excitation at room temperature. (Excitation spectra for La_2O_2S: Tb provided by PTL).

Figure 6 Emission intensities against various dopant concentrations for La_2O_2S: Tb.

Figure 7 Spectra emission distribution for La_2O_2S: Eu at dopant concentrations of 1 m/o and 7.36 m/o at room temperature. (Excitation spectra for La_2O_2S: Eu provided by PTL). Figure 7b (inset) – zoomed in on 450-500nm to indicate 467 nm and 495 nm peaks at low concentration.

Figure 8 Intensity levels of different dopant concentrations of La_2O_2S: Eu at short wavelengths.

Figure 9 Decay time against temperature for various dopant concentrations of La_2O_2S:

Eu at (a) 467 nm, (b) 495 nm, (c) 512 nm and (d) 538 nm.

Figure 10 Decay curves of La_2O_2S: 15% Tb at 544 nm line from 5- 60°C. (Refer to Figure 11 for decay time against temperature.)

Figure 11 Decay time of lower La_2O_2S: Tb concentrations (0.005 – 0.5 m/o) and higher Tb concentrations (2-50 m/o) at 544 nm as a function of temperature.

Tables

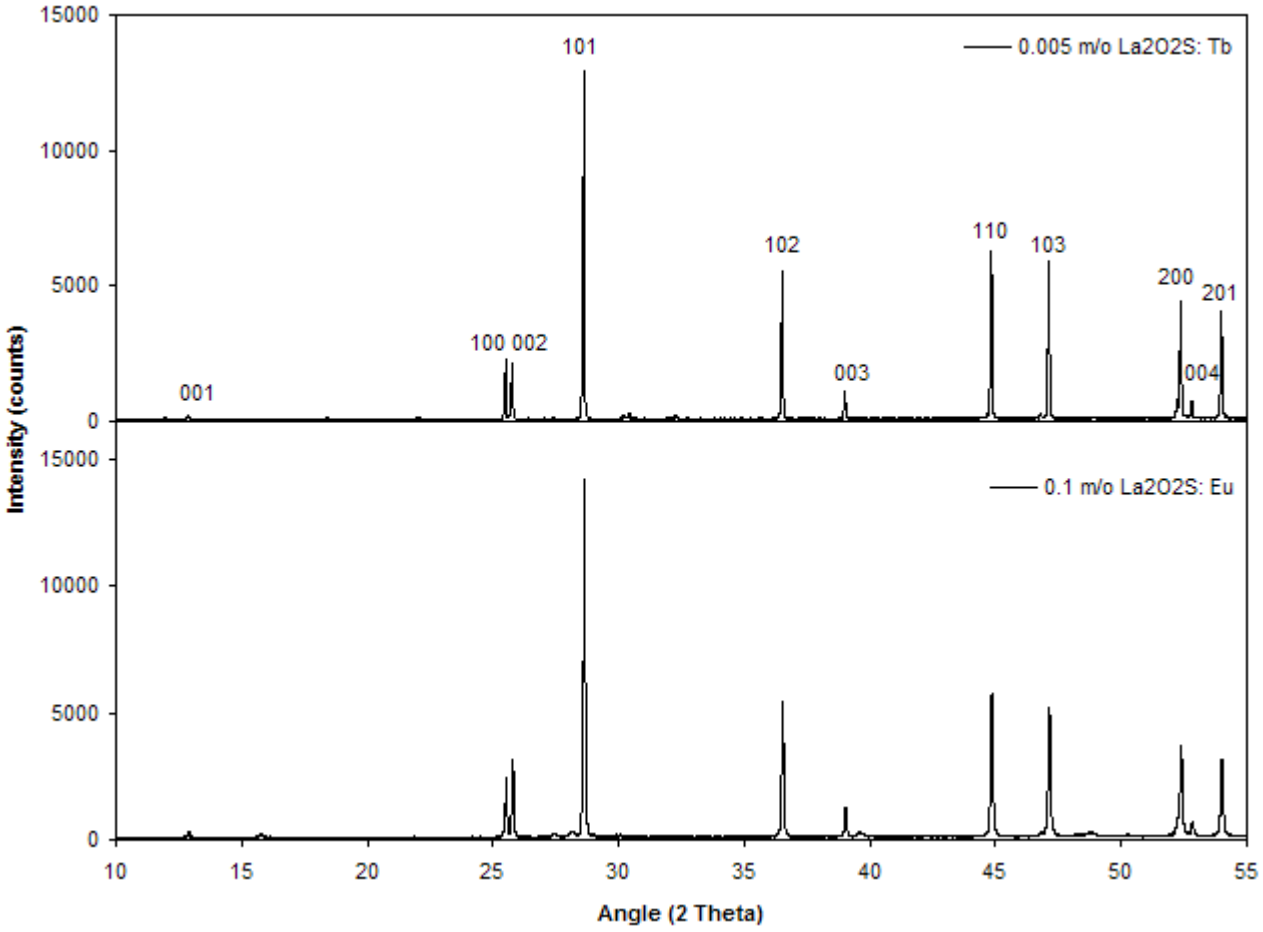

Figure 1 XRD patterns of La_2O_2S: Tb and of La_2O_2S: Eu at room temperature.

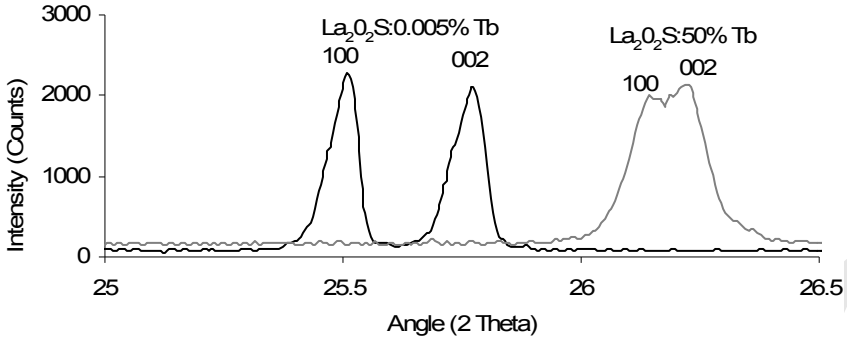

Figure 2 XRD patterns at 0.005% and 50% Tb dopancy levels over $25° \leq 2\theta \leq 26.5°$.

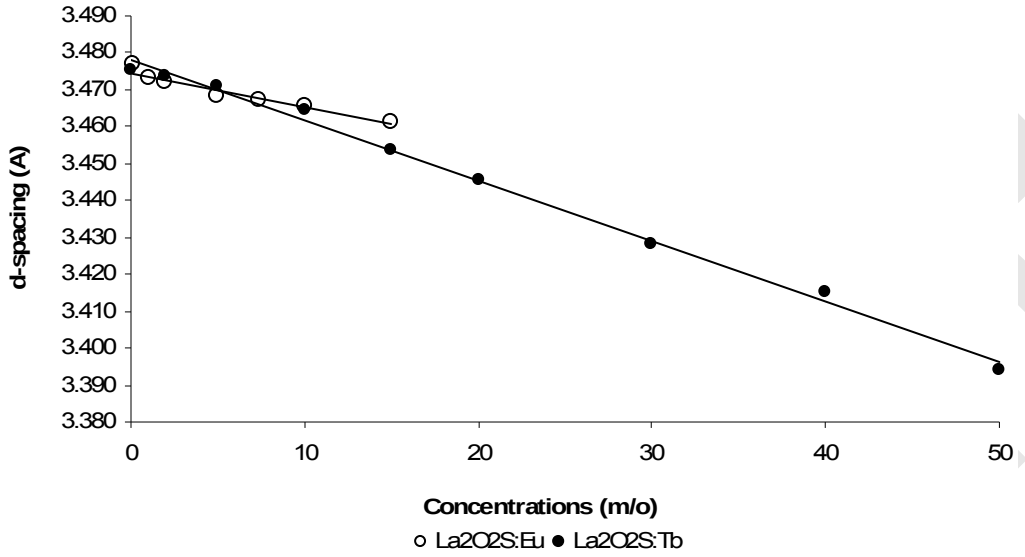

Figure 3 *C*-parameter of a unit cell of La_2O_2S: Tb and La_2O_2S: Eu as a function of dopant concentration at (002) reflection.

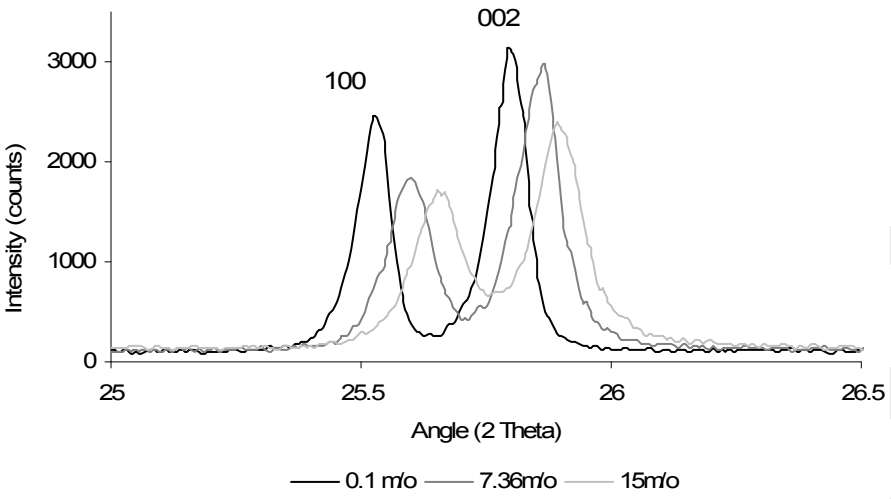

Figure 4 XRD patterns of La_2O_2S: Eu at different dopancy levels.

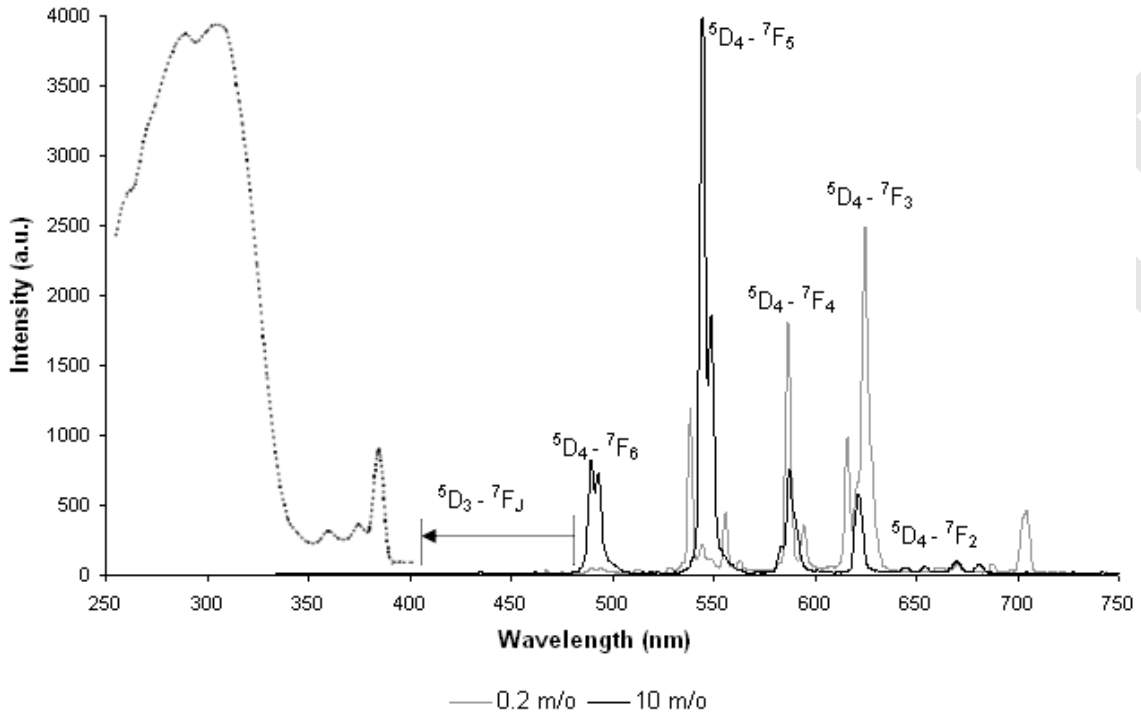

Figure 5 Emission spectra comparison of La_2O_2S: Tb at 0.2 m/o and 10 m/o Tb contents under 337 nm excitation at room temperature. (Excitation spectra for La_2O_2S: Tb provided by PTL).

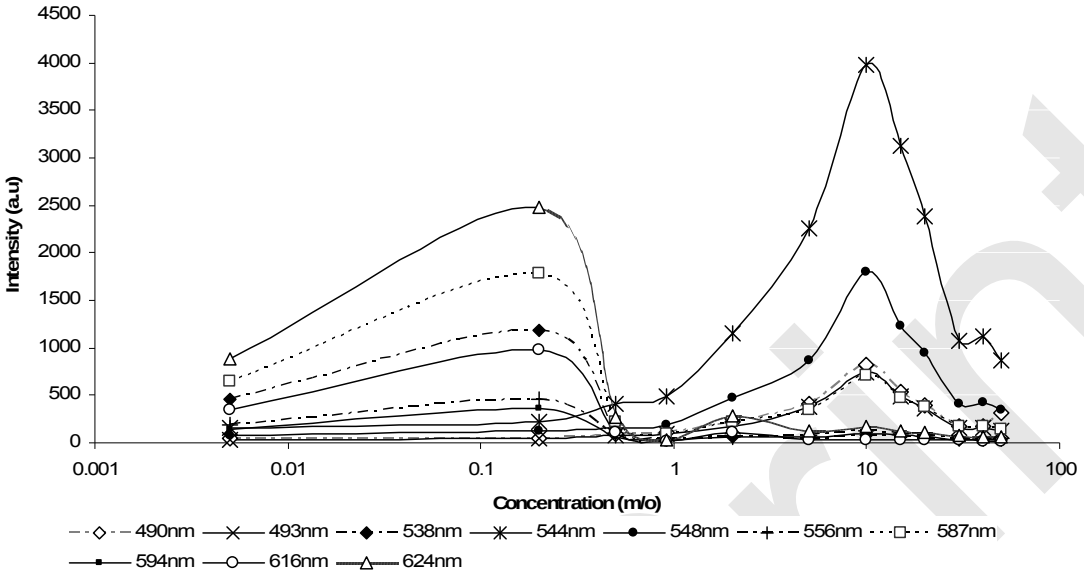

Figure 6 Emission intensities against various dopant concentrations for La_2O_2S: Tb.

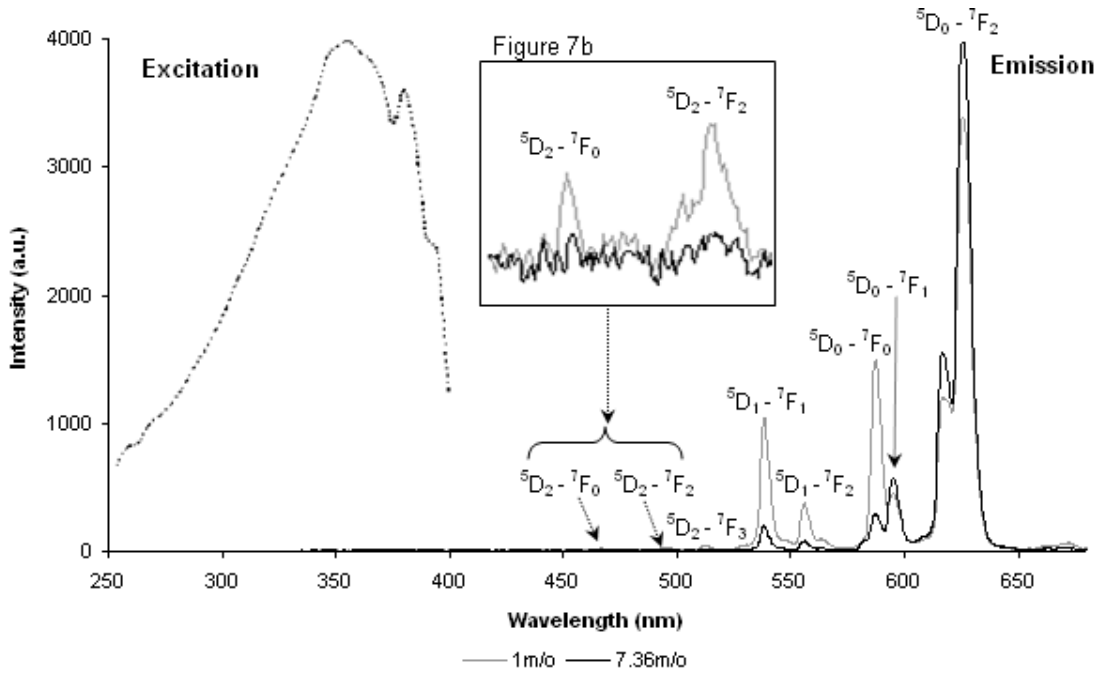

Figure 7 Spectra emission distribution for La_2O_2S: Eu at dopant concentrations of 1 m/o and 7.36 m/o at room temperature. (Excitation spectra for La_2O_2S: Eu provided by PTL). Figure 7b (inset) – zoomed in on 450-500nm to indicate 467 nm and 495 nm peaks at low concentration.

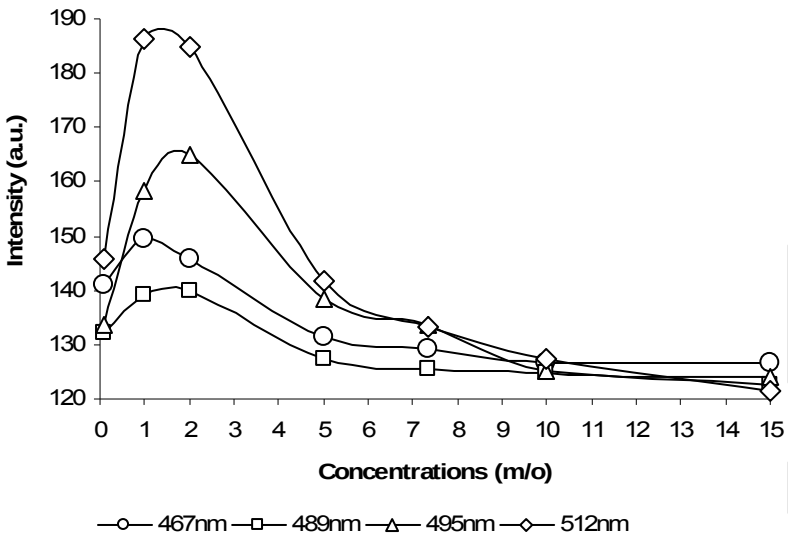

Figure 8 Intensity levels of different dopant concentrations of La_2O_2S: Eu at short wavelengths.

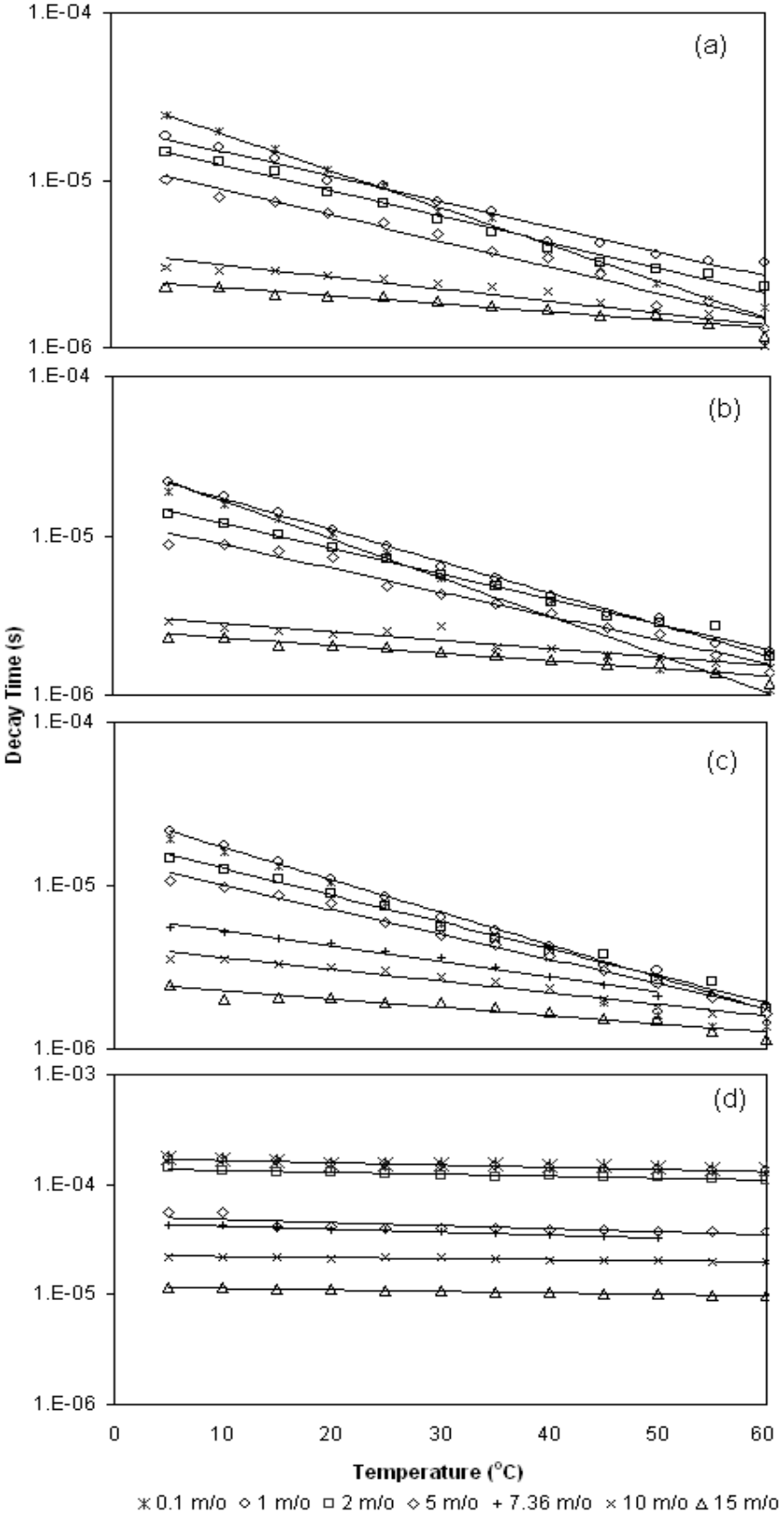

Figure 9 Decay time against temperature for various dopant concentrations of La_2O_2S: Eu at (a) 467 nm, (b) 495 nm, (c) 512 nm and (d) 538 nm.

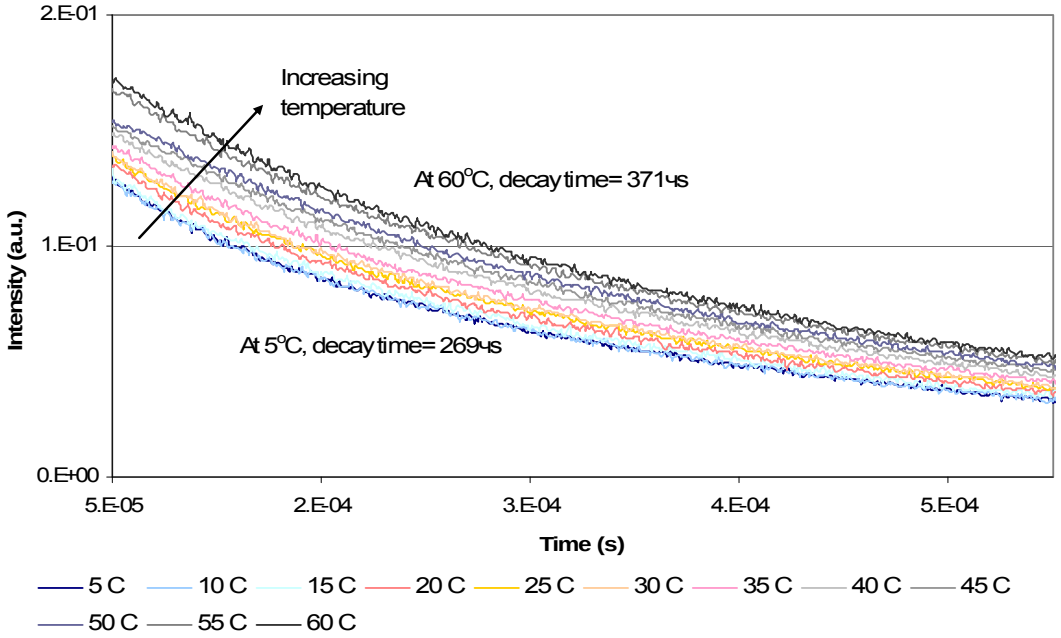

Figure 10 Decay curves of La_2O_2S: 15% Tb at 544 nm line from 5- 60°C. (Refer to Figure 11 for decay time against temperature.)

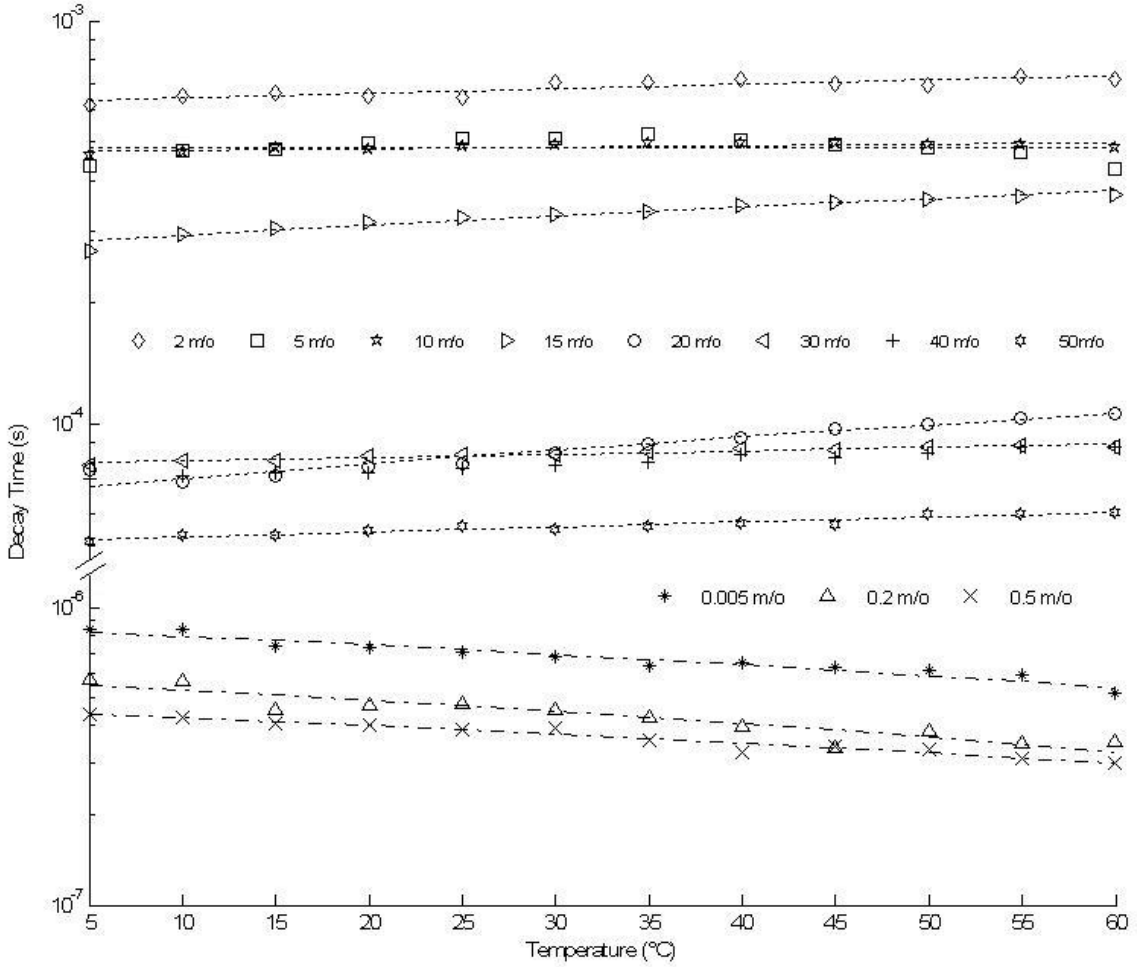

Figure 11 Decay time of lower La_2O_2S: Tb concentrations (0.005 – 0.5 m/o) and higher Tb concentrations (2-50 m/o) at 544 nm as a function of temperature.